Cryogenics 61 (2014) 70–78

Contents lists available at ScienceDirect

Cryogenics

journal homepage: www.elsevier.com/locate/cryogenics

Two dimensional model for multistream plate fin heat exchangers

Mukesh Goyal [a,b], Anindya Chakravarty [a], M.D. Atrey [b,*]

[a] Cryo-Technology Division, Bhabha Atomic Research Centre, Trombay, Mumbai 400085, India

[b] Mechanical Engineering Department, Indian Institute of Technology Bombay, Mumbai 400076, India

ARTICLE INFO

Article history:
Received 21 November 2013
Received in revised form 25 February 2014
Accepted 25 February 2014
Available online 5 March 2014

Keywords:
Plate fin heat exchanger
Helium liquefier
Helium refrigerator

ABSTRACT

A model based on finite volume analysis is presented here for multistream plate fin heat exchangers for cryogenic applications. The heat exchanger core is discretised in both the axial and transverse directions. The model accounts for effects of secondary parameters like axial heat conduction through the heat exchanger metal matrix, parasitic heat in-leak from surroundings, and effects of variable fluid properties/metal matrix conductivity. Since the fins are discretised in the transverse direction, the use of a fin efficiency is eliminated and the effects of transverse heat conduction/stacking pattern can be taken care of. The model is validated against results obtained using commercially available software and a good agreement is observed. Results from the developed code are discussed for sample heat exchangers.

1. Introduction

Plate fin heat exchangers (PFHE) having very high effectiveness (>0.95) are employed in modern helium liquefaction/refrigeration systems. A strong dependence of the helium liquefier performance on the effectiveness of heat exchangers is shown by Atrey [1]. High effectiveness, low pressure drop, compactness and design flexibility are key features of a PFHE. The performance of a PFHE, such as those employed in helium refrigeration/liquefaction systems, depends on various secondary parameters apart from basic fluid film resistances. These secondary parameters include axial heat conduction (AHC) through the heat exchanger metal matrix, parasitic heat in-leak from surroundings, variation in fluid/metal properties and flow mal-distribution. Heat exchangers have traditionally been designed and rated with lumped parameter models i.e. the logarithmic mean temperature difference (LMTD) method, the effectiveness-number of transfer units (ε-NTU) method, and so on. Treatment on these methods is available in standard text books [2–4]. These models, which represent heat exchanger basic design theory, are based on the integration of differential energy balance equations of two single phase streams under the assumptions of steady state, no heat transfer from surroundings, negligible longitudinal (axial) heat conduction, constant overall heat transfer coefficient and constant heat capacity of both the streams. Due to the above mentioned assumptions, classical closed form solutions, such as the LMTD and ε-NTU methods, cannot take care of secondary parameters.

Effects of individual secondary parameters on heat exchanger performance have been studied by many authors [5–21]. Combined effects of two or more of these parameters are also reported in some of the articles. A review on these articles is presented by Pacio and Dorao [22]. To study these combined effects, numerical methods become unavoidable, even for two-stream heat exchangers. A numerical model is presented by Nellis [23] which includes axial heat conduction, parasitic heat loads, and property variations. In this model, the heat exchanger is discretised in the axial direction and discretised energy balance equations are solved. In the case of a two-stream PFHE, due to the symmetrical temperature distribution in the fin, an adiabatic plane passing through the centre of the fin can be assumed and a fin efficiency can be used to calculate a secondary heat transfer area. In such cases, Nellis's model can be effectively used for analysis of a PFHE.

Two-stream heat exchanger analysis has been extended in the literature [24–28] for multistream heat exchangers under idealised conditions neglecting the earlier mentioned secondary parameters. In the case of two-stream heat exchangers, heat transfer occurs between neighboring passages of the hot and cold streams. Multistream PFHEs employ more than two fluid streams. Based on the stacking pattern of the streams, different passages of each stream would exhibit individual temperature profiles. There can also be transverse heat conduction through the fins. Available thermal design methodologies for multistream heat exchangers have been reviewed in detail by Das and Ghosh [29]. Most of the multistream heat exchanger design methodologies, available in the literature, are based on various assumptions. These include constant wall temperature [30–32], identical passage behavior [33], half fin length [30–32,34], area splitting [35–37], etc. Some of the earlier

* Corresponding author. Tel.: +91 22 25767522; fax: +91 22 2572 6875.
E-mail address: matrey@me.iitb.ac.in (M.D. Atrey).

http://dx.doi.org/10.1016/j.cryogenics.2014.02.017
0011-2275/

Nomenclature

$A_{b(i)}$	primary heat transfer area per unit length in the ith layer, m
$A_{b(n)}$	primary heat transfer area per unit length in the nth layer, m
$A_{f(i)}$	secondary heat transfer area per unit length in the ith layer, m
d	hydraulic diameter, m
f	Fanning friction factor
G	mass velocity, kg/m^2 s
h	heat transfer coefficient, W/m^2 K
k	thermal conductivity, W/m K
m	mass flow rate, kg/s
L	length of heat exchanger code, m
n_{axial}	number of elements in axial direction
n_{fin}	number of elements in fins in the transverse direction
$n_{lateral}$	total number of nodes in the transverse direction
n_{layers}	number of layers
$n_{streams}$	number of streams
P	pressure, Pa
Q_{conv}	heat transfer rate due to convection, W
Q_r	heat transfer rate per unit area due to radiation, W/m^2
T	temperature, K
w	width, m
w_{core}	core width, m
$w_{fin(i)}$	effective fin width in the ith layer, m
$w_{fin(n)}$	effective fin width in the nth layer, m
w_{sb}	side bar width, m
ε	effective emissivity
ρ	density, kg/m^3
σ	Stefan Boltzmann constant, W/m^2 K^4

Subscripts

P	central grid point under consideration
E, N, S, W	neighbor grid points
e, n, s, w	control volume faces
$ep1$	top end plate
$ep2$	bottom end plate
f	fluid
fin	fin
i	layer number variable
sp	separating plate
sb	side bar
∞	environment
(n)	layer number

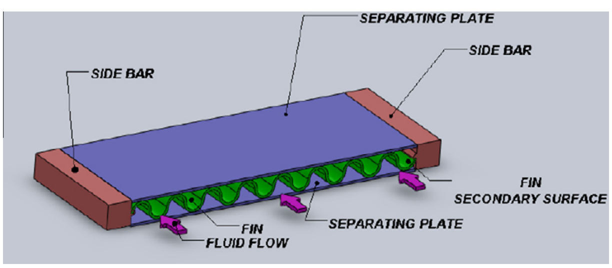

Fig. 1. Basic components of a plate fin heat exchanger.

mentioned secondary parameters have been ignored in many articles [31–35,37–44]. However, as mentioned earlier, in many applications such as in cryogenic conditions, these cannot be ignored and have to be dealt with while designing such heat exchangers.

Aspen MUSE™ [45], which is a proprietary, costly and limited period licensed commercial software available for design and rating of multistream plate fin heat exchangers, uses proprietary correlations for j–f factors of fins. In this software, fins are not discretised in the lateral direction, instead normal fin efficiency and bypass fin efficiency terms are used. Haseler [30] introduced bypass fin efficiency concept but its derivation did not include axial heat conduction.

To take care of transverse heat conduction, it is appropriate to discretise the heat exchanger in the transverse direction also. In this case, the use of a fin efficiency can be eliminated and discretised 2-D energy balance equations for fin elements can be solved. In the present paper, a numerical model, which explicitly accounts for secondary parameters like AHC through the heat exchanger metal matrix, parasitic heat in-leak from surroundings, and variable fluid properties/metal matrix conductivity, is presented for a multistream PFHE. Based on this model, a numerical tool is developed for rating calculations of a PFHE with special reference to helium cryogenic systems where one layer is confined to one fluid stream. The numerical model is validated against results obtained using Aspen MUSE™. The model is further applied to study lateral thermal profiles in multistream PFHEs using sample heat exchangers.

2. Numerical model and governing equations

Following assumptions have been made in the numerical model and in deriving discretised energy balance equations:

i. The entire heat exchanger is under steady state conditions.
ii. Variations of fluid temperature, heat transfer coefficient and friction factor perpendicular to the flow direction at a particular cross-section in any passage is negligible. Heat transfer coefficient and friction factor correlations used in the present model are also based on these assumptions.
iii. Temperature variations across the thickness of the fin is negligible due to thin fins.
iv. The metal matrix temperature inside the core is constant along the width of the heat exchanger, but this temperature is different than the temperature of the side bars. In high effectiveness PFHEs for cryogenic applications, the fin density is large and the assumption of constant temperature along the core width can be justified. Due to comparatively thick side bars, there may be large lateral (transverse) heat conduction through the side bars resulting into a different lateral temperature profile in the side bars compared to the inside core.
v. Heat conduction through the gas is neglected in comparison to the heat conduction through the metal.
vi. Flow mal-distribution is neglected.
vii. The effect of pressure drop on the heat transfer calculations is neglected.

2.1. Model description

A PFHE is a type of compact heat exchanger which consists of stacks of alternate layers of corrugated die-formed metal sheets (the fins) separated by flat metal separation sheets (the plates). The basic components of a PFHE are shown in Fig. 1.

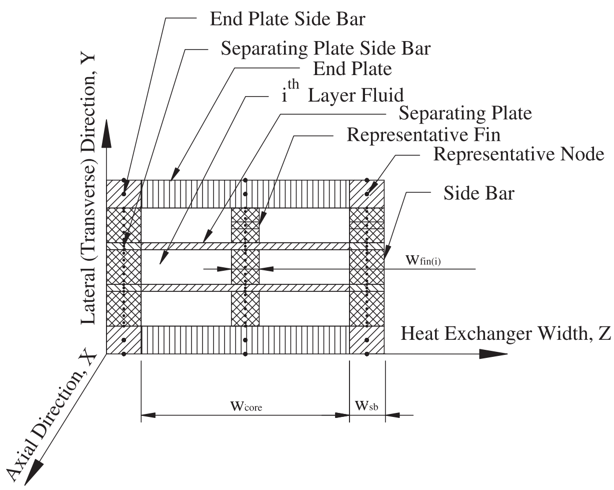

Fig. 2. Simplified cross-sectional model of a sample PFHE with 3 layers.

Fig. 2 describes a simplified cross-sectional model of a sample PFHE with three layers. From the earlier mentioned assumptions (iii) and (iv), every fin in a layer at a particular cross-section shows a similar thermal behavior and temperature profile. Therefore, it is possible to represent the fins in a particular layer through one equivalent fin with a thickness equal to the total fin thickness and a heat transfer area equal to the total heat transfer area of all the fins. The fins (and side bars) are divided in the lateral direction in n_{fin} elements. The heat exchanger is divided in the axial direction in n_{axial} elements. In the lateral direction, 3 nodes are placed in each separating plate/end plate. The total number of lateral nodes for core elements is $n_{lateral}$, the same as that used for side bars.

2.2. Discretised energy balance equations

In each of the volume elements of the metal matrix, there exists 2-D heat conduction (along the length of heat exchanger and along the lateral direction as represented by direction X and direction Y respectively in Fig. 2).

Energy balance equations for these elements can be represented as steady two dimensional heat conduction governed by the following general equation:

$$\frac{\partial}{\partial x}\left(k\frac{\partial T}{\partial x}\right)+\frac{\partial}{\partial y}\left(k\frac{\partial T}{\partial y}\right)+S=0 \quad (1)$$

where S is the source term which takes a different form for different components of the heat exchanger.

Discretised energy balance equations for each volume element are derived in finite difference form. The nomenclature for grid points and interfaces are similar to that used by Patankar [46]. Due to the 2-D discretisation of the domain, it is possible to explicitly incorporate AHC, variable fluid/metal properties, parasitic heat in-leak from surroundings and transverse heat conduction.

The following heat transfer terms are taken into consideration in the discretised energy balance equations.

(a) Convective heat transfer to the fluid and conductive heat transfer to the fins at the inner surface of end plates and both surfaces of separating plates.
(b) Convective heat transfer to the fluid from inner surfaces of side bars.
(c) Parasitic heat in-leak from surroundings to the outer surfaces of the heat exchanger. This term is taken in the form of radiation with an effective emissivity term and can be represented as:

$$Q_r=\sigma\epsilon(T_\infty^4-T_P^4) \quad (2)$$

where Q_r is radiative heat in-leak per unit area.

Zero thickness elements are taken at the boundary of the heat exchanger components to take care of the boundary conditions.

The Left Boundary Condition (Hot End) at $X = 0$ can be expressed as:

$$T_P=\frac{Q_r dx}{2k_P}+T_E \quad (3)$$

The Right Boundary Condition (Cold End) at $X = L$ is given by:

$$T_P=\frac{Q_r dx}{2k_P}+T_W \quad (4)$$

2.2.1. Energy balance equations for fins

The computational grid of a representative fin in the ith layer is shown in Fig. 3. There are $(n_{fin}\times n_{axial})$ volume elements in each fin. The source term S, for the fin elements, consists of heat convected from the fin elements to the fluid elements. From the discretised energy balance equations of the fin elements, the central grid point temperature T_p can be represented as:

$$T_P=\frac{\frac{k_n dx}{dy_n}T_N+\frac{k_s dx}{dy_s}T_S+\frac{k_e dy_{fin(i)}}{dx_e}T_E+\frac{k_w dy_{fin(i)}}{dx_w}T_W+\frac{hA_{f(i)}dx}{n_{fin}w_{fin(i)}}T_f}{\frac{k_n dx}{dy_n}+\frac{k_s dx}{dy_s}+\frac{k_e dy_{fin(i)}}{dx_e}+\frac{k_w dy_{fin(i)}}{dx_w}+\frac{hA_{f(i)}dx}{n_{fin}w_{fin(i)}}} \quad (5)$$

2.2.2. Energy balance equations for side bars

There are $(n_{fin}\times n_{axial})$ volume elements in each side bar. The source term S, for the side bar elements, consists of heat convected from the inner surfaces of the side bars to the fluid elements and heat radiated from surroundings to the outer surfaces of side bars. Using discretised energy balance equations of the side bar elements, the central grid point temperature T_p can be written as:

$$T_P=\frac{\frac{k_n dx w_{sb}}{dy_n}T_N+\frac{k_s dx w_{sb}}{dy_s}T_S+\frac{k_e dy_{fin(i)}w_{sb}}{dx_e}T_E+\frac{k_w dy_{fin(i)}w_{sb}}{dx_w}T_W+Q_r dy_{fin(i)}dx+h dy_{fin(i)}dx T_f}{\frac{k_n dx w_{sb}}{dy_n}+\frac{k_s dx w_{sb}}{dy_s}+\frac{k_e dy_{fin(i)}w_{sb}}{dx_e}+\frac{k_w dy_{fin(i)}w_{sb}}{dx_w}+h dy_{fin(i)}dx} \quad (6)$$

2.2.3. Energy balance equations for end plates and separating plates

Along the width of the heat exchanger, there is no temperature gradient inside the heat exchanger core, but the core temperature is different than the side bar temperature, as described in the assumption (iv). Since the side bar temperature is different than that in the heat exchanger core, heat is conducted from the side bars to the separating plates and the end plates in the Z direction. The source term S, for the separating plate/end plate elements and the corresponding side bar elements, consists of heat conducted between the side bar elements and the separating plate/end plate elements.

2.2.4. Energy balance equations for end plates

The computational grid of the bottom end plate is shown in Fig. 4. Heat conducted from each of the side bars to the bottom

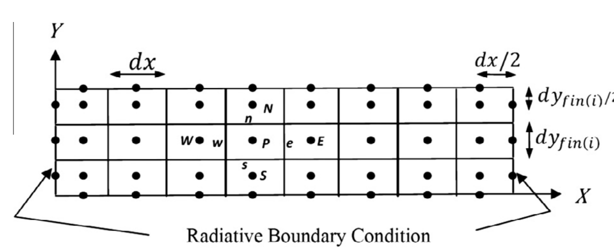

Fig. 3. Computational grid of a representative fin in layer i.

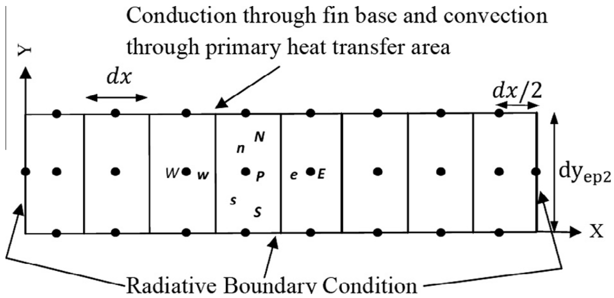

Fig. 4. Computational grid of bottom end plate.

end plate (ep_2) elements in the Z direction (as shown in Fig. 2) can be represented as:

$$Q_{cond,Z} = \frac{dxdy_{ep2}}{(w_{sb}/2)} k_p (T_{sb} - T_p) \tag{7}$$

Using discretised energy balance equations for the bottom end plate elements, the central grid point temperature T_p can be written as:

$$T_P = \frac{\frac{w_{core}dx}{dy_n} k_n T_N + \frac{w_{core}dx}{dy_s} k_s T_S + \frac{w_{core}dy_{ep2}}{dx_e} k_e T_E + \frac{w_{core}dy_{ep2}}{dx_w} k_w T_W + \frac{2dxdy_{ep2}}{(w_{sb}/2)} k_p T_{sb}}{\frac{w_{core}dx}{dy_n} k_n + \frac{w_{core}dx}{dy_s} k_s + \frac{w_{core}dy_{ep2}}{dx_e} k_e + \frac{w_{core}dy_{ep2}}{dx_w} k_w + \frac{2dxdy_{ep2}}{(w_{sb}/2)} k_p} \tag{8}$$

Since there are two side bars (one at each side), cross-sectional area for conduction from the side bars to the end plate is $2dxdy_{ep2}$. Nodal separation distance between T_{sb} and T_p is $w_{sb}/2$. Here, w_{sb} is the side bar width and T_{sb} is the central node temperature of the side bar element. As per the assumption (iv) of the numerical model, the metal matrix temperature inside the core is constant along the width of the heat exchanger, therefore, T_p is constant along the Z-direction for the end plate. W_{core}, is the width of the end plate. In general, k_p is the thermal conductivity of the central node under consideration and its value is taken from the previous iteration. k_p, in this case, represents thermal conductivity of the bottom end plate.

The temperature at the bottom boundary nodes can be expressed as:

$$T_P = \frac{Q_r dy_{ep2}}{2k_P} + T_N \tag{9}$$

The temperature at the top boundary nodes is given by:

$$T_P = \frac{\frac{2w_{fin(n)}}{dy_{fin(n)}} k_P T_N + \frac{2w_{core}}{dy_{ep2}} k_P T_S + h\frac{A_{b(n)}}{2} T_f}{\frac{2w_{fin(n)}}{dy_{fin(n)}} k_P + \frac{2w_{core}}{dy_{ep2}} k_P + h\frac{A_{b(n)}}{2}} \tag{10}$$

Discretised energy balance equations for the top end plate elements can be obtained in similar fashion.

2.2.5. Energy balance equations for end plate side bars

Using discretised energy balance equations for the bottom end plate side bar elements, the central grid point temperature T_p can be written as:

$$T_P = \frac{\frac{w_{sb}dx}{dy_n} k_n T_N + \frac{w_{sb}dx}{dy_s} k_s T_S + \frac{w_{sb}dy_{ep2}}{dx_e} k_e T_E + \frac{w_{sb}dy_{ep2}}{dx_w} k_w T_W + \frac{dxdy_{ep2}}{(w_{sb}/2)} k_{ep2} T_{ep}}{\frac{w_{sb}dx}{dy_n} k_n + \frac{w_{sb}dx}{dy_s} k_s + \frac{w_{sb}dy_{ep2}}{dx_e} k_e + \frac{w_{sb}dy_{ep2}}{dx_w} k_w + \frac{dxdy_{ep2}}{(w_{sb}/2)} k_{ep2}} \tag{11}$$

The temperature at the bottom boundary nodes can be expressed as:

$$T_P = \frac{Q_r dy_{ep2}}{2k_P} + T_N \tag{12}$$

The temperature at the top boundary nodes is given by:

$$T_P = \frac{\frac{1}{dy_{fin(n)}} T_N + \frac{1}{dy_{ep2}} T_S}{\frac{1}{dy_{fin(n)}} + \frac{1}{dy_{ep2}}} \tag{13}$$

Discretised energy balance equations for the top end plate side bar elements can be obtained in similar fashion.

2.2.6. Energy balance equations for separating plates

Heat conducted from each of the side bars to the ith separating plate elements in the Z direction (as shown in Fig. 2) can be represented as:

$$Q_{cond,Z} = \frac{dxdy_{sp(i)}}{(w_{sb}/2)} k_p (T_{sb} - T_p) \tag{14}$$

Using discretised energy balance equations for the ith separating plate elements, the central grid point temperature T_p can be written as:

$$T_P = \frac{\frac{k_n dx w_{core}}{dy_n} T_N + \frac{k_s dx w_{core}}{dy_s} T_S + \frac{k_e dy_{sp(i)} w_{core}}{dx_e} T_E + \frac{k_w dy_{sp(i)} w_{core}}{dx_w} T_W + \frac{2dxdy_{sp(i)}}{(w_{sb}/2)} k_p T_{sb}}{\frac{k_n dx w_{core}}{dy_n} + \frac{k_s dx w_{core}}{dy_s} + \frac{k_e dy_{sp(i)} w_{core}}{dx_e} + \frac{k_w dy_{sp(i)} w_{core}}{dx_w} + \frac{2dxdy_{sp(i)}}{(w_{sb}/2)} k_p} \tag{15}$$

Details of various terms appearing in Eq. (15) have been given after Eq. (8). However, in the present case, as against bottom end plate considered in Eq. (8), separating plate is considered.

The temperature at the top boundary nodes can be expressed as:

$$T_P = \frac{\frac{2k_P w_{fin(i)}}{dy_{fin(i)}} T_N + \frac{2k_P w_{core}}{dy_{sp(i)}} T_S + \frac{hA_{b(i)}}{2} T_f}{\frac{2k_P w_{fin(i)}}{dy_{fin(i)}} + \frac{2k_P w_{core}}{dy_{sp(i)}} + \frac{hA_{b(i)}}{2}} \tag{16}$$

The temperature at the bottom boundary nodes is given by:

$$T_P = \frac{\frac{2k_P w_{core}}{dy_{sp(i)}} T_N + \frac{2k_P w_{fin(i+1)}}{dy_{fin(i+1)}} T_S + \frac{hA_{b(i+1)}}{2} T_f}{\frac{2k_P w_{core}}{dy_{sp(i)}} + \frac{2k_P w_{fin(i+1)}}{dy_{fin(i+1)}} + \frac{hA_{b(i+1)}}{2}} \tag{17}$$

2.2.7. Energy balance equations for separating plate side bars

Using discretised energy balance equations for the ith separating plate side bar elements, the central grid point temperature T_p can be written as:

$$T_P = \frac{\frac{k_n dx w_{sb}}{dy_n} T_N + \frac{k_s dx w_{sb}}{dy_s} T_S + \frac{k_e dy_{sp(i)} w_{sb}}{dx_e} T_E + \frac{k_w dy_{sp(i)} w_{sb}}{dx_w} T_W + \frac{2dxdy_{sp(i)}}{(w_{sb}/2)} k_{sp} T_{sp} + Q_r dxdy_{sp(i)}}{\frac{k_n dx w_{sb}}{dy_n} + \frac{k_s dx w_{sb}}{dy_s} + \frac{k_e dy_{sp(i)} w_{sb}}{dx_e} + \frac{k_w dy_{sp(i)} w_{sb}}{dx_w} + \frac{2dxdy_{sp(i)}}{(w_{sb}/2)} k_{sp}} \tag{18}$$

The temperature at the top boundary nodes can be expressed as:

$$T_P = \frac{\frac{1}{dy_{fin(i)}} T_N + \frac{1}{dy_{sp(i)}} T_S}{\frac{1}{dy_{fin(i)}} + \frac{1}{dy_{sp(i)}}} \tag{19}$$

The temperature at the bottom boundary nodes is given by:

$$T_P = \frac{\frac{1}{dy_{sp(i)}} T_N + \frac{1}{dy_{fin(i+1)}} T_S}{\frac{1}{dy_{sp(i)}} + \frac{1}{dy_{fin(i+1)}}} \tag{20}$$

2.2.8. Energy balance equations for fluids

The energy balance equation for the fluid elements in the ith layer for the positive flow direction can be written as:

$$m_i C_{pi,T_{favg}} (T_{f(i,j)} - T_{f(i,j+1)}) = Q_{conv} \tag{21}$$

where,

$$Q_{conv} = Q_{sp} + Q_{fin} + Q_{sb} \tag{22}$$

$$Q_{conv} = h\frac{A_{b(i)}}{2}dx(2T_{f_{avg}} - metalArr_{(3i+n_{fin}(i-1),j+1)} - metalArr_{(1+(n_{fin}+3)i,j+1)})$$
$$+\sum_{k=1}^{n_{fin}}\left[h\frac{A_{f(i)}}{n_{fin}}dx(T_{f_{avg}} - metalArr_{(3i+n_{fin}(i-1)+k,j+1)}) + 2hdy_{fin(i)}dx \times \left(T_{f_{avg}}\, metalArr_{(3i+n_{fin}(i-1)+k+n_{lateral},j+1)}\right)\right] \quad (23)$$

Here, the *metalArr* is a 2-D metal temperature matrix and j represents axial node number. In the *metalArr*, there are $(2 \times n_{lateral})$ rows and $(n_{axial} + 2)$ columns. First $n_{lateral}$ rows of the *metalArr* represent core temperatures and next $n_{lateral}$ rows represent side bars. In the ith layer, $metalArr_{(3i+nfin(i-1),j+1)}$ represents top separating plate surface in contact with the fluid, $metalArr_{(1+(nfin+3)i,j+1)}$ represents bottom separating plate surface in contact with the fluid, $metalArr_{(3i+nfin(i-1)+k,j+1)}$ represents fin elements and $metalArr_{(3i+nfin(i-1)+k+n_{lateral},j+1)}$ represents side bar elements. $T_{f_{avg}}$ is the average fluid temperature of the ith layer fluid element under consideration and is equal to $\frac{T_{f(i,j+1)}+T_{f(i,j)}}{2}$.

The fluid temperature for the positive flow direction can be expressed as:

$$T_{f(i,j+1)} = T_{f(i,j)} - \frac{Q_{conv}}{m_i C_{pi,T_{f_{avg}}}} \quad (24)$$

The fluid temperature for the negative flow direction is given by:

$$T_{f(i,j)} = T_{f(i,j+1)} - \frac{Q_{conv}}{m_i C_{pi,T_{f_{avg}}}} \quad (25)$$

The core pressure drop in the ith layer consists of two components, the frictional pressure drop and the pressure drop (or rise) due to the rate of change of momentum. This can be expressed as [2]:

$$\Delta P_i = \frac{G^2}{2}\left[\sum_{j=1}^{n_{axial}}\frac{4dx}{d}(f/p)_{T_f} + 2\left(\frac{1}{\rho_{exit}} - \frac{1}{\rho_{in}}\right)\right] \quad (26)$$

3. Solution technique

The system of discretised energy balance equations is solved iteratively using reasonable initial guesses with suitable relaxation factors for metal and fluid nodes. Fig. 5 describes the flow chart of the solution algorithm. The numerical technique, as described above, is implemented through visual basic. The computer program uses MSEXCEL® for user interaction. Thermo-physical properties of the fluids are evaluated using GASPAK® [47]/HEPAK® [48]. The thermal conductivity of Aluminium (Al) (Construction material selected for heat exchanger) is evaluated using an empirical correlation from NIST [49]. Heat transfer coefficient/friction factor correlations [50] for offset strip fins are used in the code, although the mathematical formulation developed and described in the earlier sections is valid for fins of different types.

4. Results and discussions

4.1. Model validation

The numerical model presented in this paper is a generalized model and can be used for rating calculations of heat exchangers with any number of streams. The dimensions of PFHE cores used for model validation and parametric studies are given in Table 1. Fig. 6 describes the serrated type fins used in the sample PFHE. For heat transfer and flow friction characteristics, well known Manglik and Bergles correlations are applied [50]. Operating conditions and process parameters used for case studies are described in

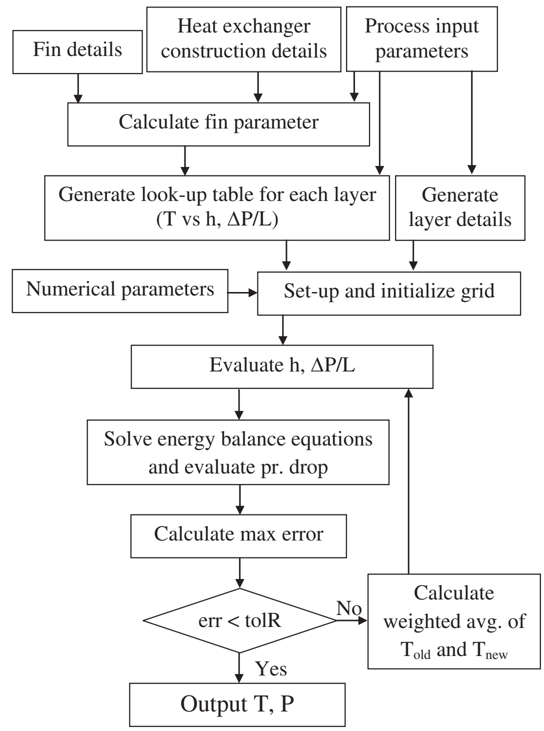

Fig. 5. Flow chart of the solution algorithm.

Table 1
Details of heat exchanger core.

Description	Case 1–3	Case 4
Heat exchanger matrix metal	Aluminium (3003)	Aluminium (3003)
Core length	1200 mm	1160 mm
Core width	184 mm	300 mm
Side bar width	8 mm	10 mm
Total width	200 mm	320 mm
Separating plate thickness	0.8 mm	0.8 mm
End plate thickness	3.8 mm	5.8 mm
Fin type	Serrated	Serrated
Fin metal thickness	0.2 mm	0.2 mm
Fin height	6.3 mm	3.6 mm
Serration length	3 mm	3 mm
Fin pitch	1.4 mm	1.4 mm

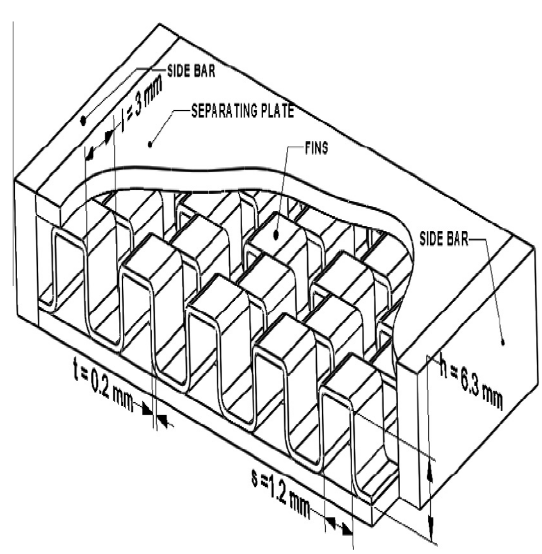

Fig. 6. Schematic of offset-strip fins.

Table 2
Operating conditions and process parameters for case studies.

Case no.	Stream no.	Working fluid	Mass flow rate (g/s)	P_{in} (MPa)	T_{in} (K)	Total no. of layers	Layer arrangement
1	1	He	10	0.210	80.00	1	1-2
	2	He	10	0.700	311.00	1	
2	1	He	10	0.210	80.00	2	1-2-1
	2	He	10	0.700	311.00	1	
3	1	He	10	0.210	80.00	1	1-2-3
	2	He	10	0.700	311.00	1	
	3	N_2	2.7	0.110	80.00	1	
4	1	He	17	1.219	43.05	6	2-3-2-3-2-1-2-3-2-3-2-1-2-3-2-3-2-1-2-3-2-3-2-1-2-3-2-1-2-3-2-3-2-1-2-3-2-3-2
	2	He	62	0.144	11.00	20	
	3	He	45	0.650	43.05	13	

Table 2. These cases are selected to cover various possibilities that exist in a helium liquefier or a refrigerator. Case-1 is a two stream He–He heat exchanger with one layer for each stream. Case-2 is also a two stream He–He heat exchanger with 2 layers for the cold stream and one layer for the hot stream which is kept in the middle. Due to symmetrical heat input, the lateral temperature profile in this case should also be symmetrical and this symmetry can be used for model validation. Case 3 is a 3-stream He–He–N_2 heat exchanger with one layer for each stream. A heat exchanger similar to Case-3 exists as the 1st heat exchanger in the helium liquefier/refrigerator with LN_2 pre-cooling arrangement. In this case, a high pressure warm helium gas stream is cooled by low pressure cold return helium gas stream and a cold N_2 vapour stream. The number of layers for all these cases is deliberately kept at a minimum, so that the lateral temperature profile could be analysed and understood in detail. Case-4 represents a realistic case of a 3 stream He–He–He heat exchanger, typically used between two turbines in modern turbine based helium liquefiers/refrigerators. In all the above cases, the pressures of the fluids are normally different.

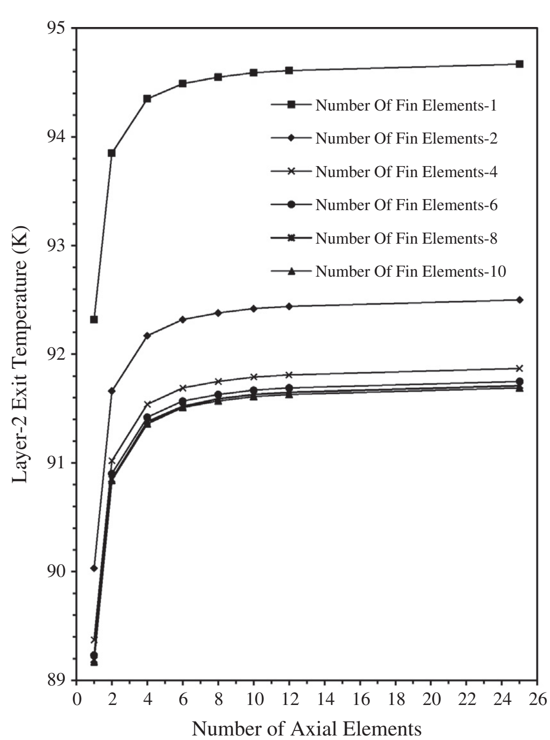

Fig. 7. Grid independence test for Case-3.

Fig. 7 demonstrates the grid independence of the code. This is done by plotting fluid exit temperatures against grid density. In the present work, this test is carried out for case-3 which is a 3-stream heat exchanger. For this test, layer-2 exit temperatures are plotted against the number of axial elements keeping the number of elements in the fins as constant. The number of elements in the fins is increased from 1 to 10, while the number of elements in the axial direction is increased from 1 to 25. It can be observed that layer-2 exit temperatures follow different curves for different number of elements in the fins. As the number of elements in the fins is increased, these curves almost merge together. This indicates grid independence of the code against grid density in the fins. It is seen that, as the number of elements in the axial direction is increased, layer-2 exit temperatures become independent of number of axial elements. This shows grid independence of the code against grid density in the axial direction. This test is carried out for all the cases described in the present work.

Results from the present code are compared with the results obtained using commercial software Aspen MUSE™ [45]. The comparison is carried out with respect to exit temperatures of the working fluids as well as fluid temperature profiles along the length of heat exchangers. Table 3 gives the comparison of the fluid outlet temperatures, while Figs. 8 and 9 give fluid temperature profiles along the length of the heat exchangers for cases 3 and 4 respectively. It is obvious from these figures and table that there exists a good agreement between the developed code and Aspen MUSE™ [45].

4.2. Lateral temperature profiles for multistream heat exchangers

The lateral temperature profile of the heat exchanger matrix and fluid at the mid axial position of the heat exchanger is shown in Figs. 10–13 for Cases 1–4 respectively.

Fig. 10 shows lateral temperature profiles for different elements of the heat exchanger matrix as described in Fig. 2 for Case-1. In this figure, the top end plate (&top end plate side bar), fin in layer-1 (& side bar), separating plate (& separating plate side bar), fin in layer-2 (& side bar), bottom end plate (&bottom end plate side bar) are represented by nodes 1–3, 3–14, 14–16, 16-27, 27–29 respectively. The fluid in layer-1 is warm helium while the fluid in layer-2 is cold helium. It may be observed that the temperature between nodes 1–2 and nodes 28–29 is constant; this is due to adiabatic end condition in the end plates (Effective emissivity in the studied cases is taken as zero). A linear temperature gradient exists between nodes 14–16, which represents the temperature drop in the separating plate due to heat conduction. It may be noted that the lateral temperature profile of the side bars is quite different than the core temperature profile. A nonlinear temperature profile can be seen in the representative fin. This is due to near adiabatic end condition at the fin end near the

Table 3
Comparison of results.

Case no.	Stream no.	T_{exit} (K)		ΔP (bar)	
		Aspen MUSE [45]	Present code	Aspen MUSE [45]	Present code
1	1	293.81	294.12	0.15640	0.15337
	2	97.27	96.91	0.04964	0.04793
2	1	298.79	298.61	0.05248	0.05149
	2	92.31	92.43	0.04882	0.04726
3	1	287.28	287.37	0.13358	0.13865
	2	91.85	91.69	0.04508	0.04344
	3	300.45	299.21	0.00546	0.00501
4	1	13.48	13.51	0.00043	0.00040
	2	41.86	41.76	0.00377	0.00371
	3	13.49	13.55	0.00104	0.00104

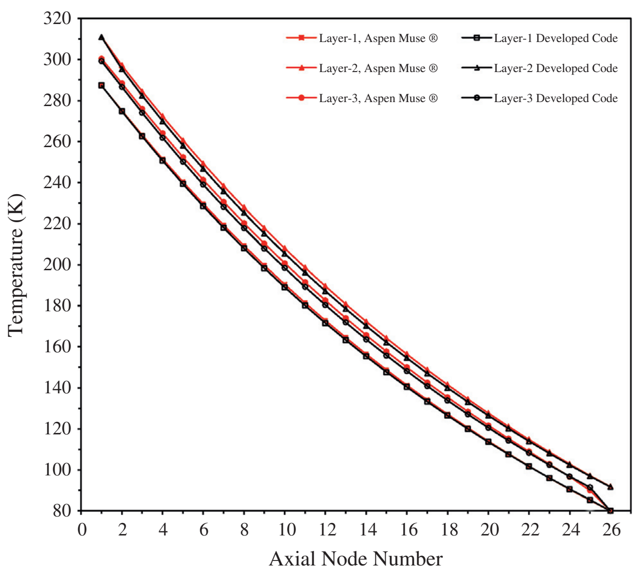

Fig. 8. Fluid temperature profile for Case-3.

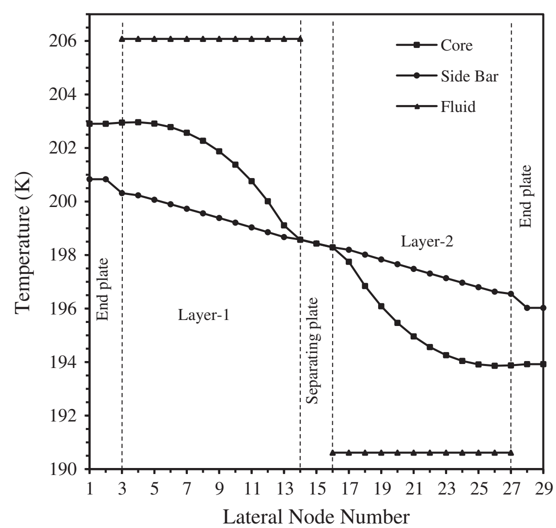

Fig. 10. Lateral temperature profile at mid axial position for Case-1.

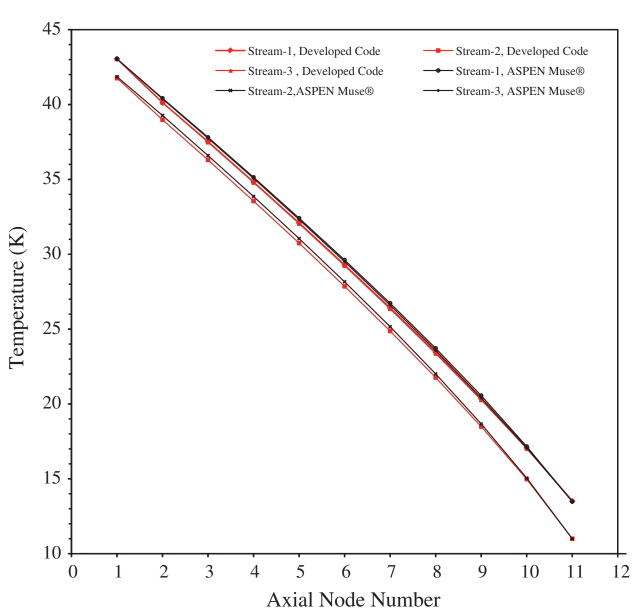

Fig. 9. Fluid temperature profile for Case-4.

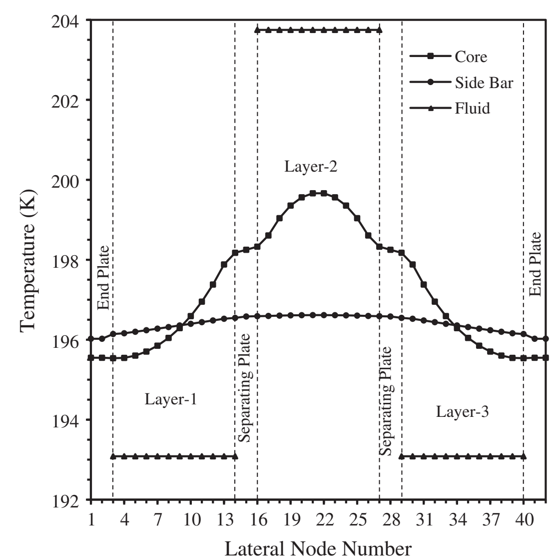

Fig. 11. Lateral temperature profile at mid axial position for Case-2.

end-plate. There exists a near linear temperature profile in the side bars. This is due to dominance of conduction heat transfer which results into transverse heat conduction between the separating plate and the end plate through the side bars.

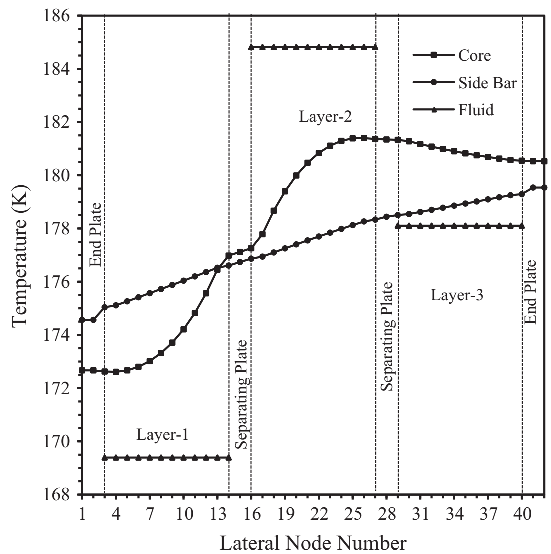

Fig. 12. Lateral temperature profile at mid axial position for Case-3.

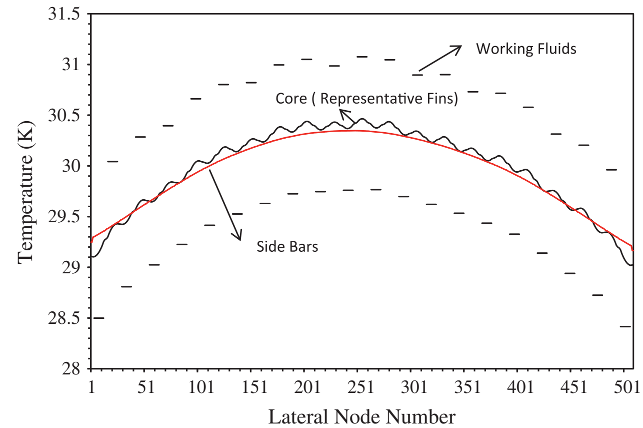

Fig. 13. Lateral temperature profile at mid axial position for Case-4.

Fig. 11 shows the lateral temperature profile for case-2. The fluid in layer-2 is warm helium while the fluid in layer-1 and 3 is cold helium. It may be seen that the lateral temperature profile is perfectly symmetrical for this case. This is due to symmetrical heat input to the central layer from the outer layers. A zero temperature gradient is observed at the middle of the fin in layer-2. For such cases, a half fin length idealization can be used instead of fin discretisation in the lateral direction. There exists no transverse heat conduction between the two separating plates. Transverse heat conduction through the side bars between the separating plates and the end plates is also negligible due to more uniformity in the metal matrix temperature.

Fig. 12 shows the lateral temperature profile for case-3. The fluid in layer-2 is warm helium which is being pre-cooled by the cold helium in layer-1 and the cold N_2 vapour in layer-3. Both the cold streams are entering at 80 K. It may be observed from Fig. 8 that there is a sharp rise in the temperature of the N_2 vapour in layer-3 at the cold end. This is due to the fact that the heat capacity of N_2 vapour in the layer-3 is less as compared to the heat capacity of cold helium in layer-1. As a result, the temperature approach between the N_2 vapour and the warm helium is smaller compared to that between the cold and warm helium streams. Due to the above mentioned reasons the lateral temperature profile in the heat exchanger matrix becomes non-symmetrical although the inlet temperatures of cold helium and N_2 vapour are the same. It can be seen that the zero temperature gradient point inside the fin in layer-2 is closer to the separating plate between layer-2 and layer-3. It may therefore be concluded that most of the fin area of layer-2 participates with layer-1 for heat transfer. In such cases, a half fin length idealisation may result in large errors and appropriate area participation factors need to be considered. In this case, transverse heat conduction through the side bars is present not only between the separating plates and end plates but also in between the separating plates. This indicates that the fluid in layer-3 interacts not only with the fluid in the layer-2 but also with the fluid in the layer-1. It may be appreciated that the temperature profile would alter based on the heat capacity ratios of the fluid streams.

Fig. 13 shows lateral temperature profile for case-4 which represents an actual heat exchanger in a helium refrigerator/liquefier. In this case, there are a total of 39 layers. The high pressure warm helium stream (6 layers) and medium pressure warm helium stream (13 layers) are cooled by the low pressure cold helium stream (20 layers). The number of layers for each stream is decided based on the required heat transfer, allowable pressure drop and limitations on overall length of the heat exchanger. There are alternate layers of warm and cold streams. The layer arrangement for this case is given in Table 2. It can be seen that all the separating plates are at different the temperatures, although the differences are small. It may be noticed that all the layers have a zero temperature gradient point inside the fins; therefore transverse heat conduction through the fins does not exist. However, transverse heat conduction from the central layers to the outer layers through the side bars does exist.

5. Conclusion

The numerical model presented here can be successfully used for rating calculations of multistream PFHE for cryogenic applications. The model takes care of various secondary parameters such as axial and transverse heat conduction, effects of variable fluid properties/metal matrix conductivity and heat in-leaks from surroundings. The model uses heat transfer and friction factor characteristics of fins available in the published literature. Due to 2-D discretisation, need of fin efficiency term is eliminated. The model is presented with detailed energy balance equations along with solution algorithm. The results obtained are in good agreement with commercially available software Aspen MUSE™ [45]. The model is very useful to compute the effect of lateral heat conduction when applied to a multistream PFHE as is shown in case-3 study. Depending on lateral temperature profiles, the model can be used to optimise stacking patterns. It may be worth highlighting that since the model is based on 2-D discretisation, it cannot take care of the temperature variations along the width of the heat exchanger. Due to this, the model cannot be used for rating of multistream plate fin heat exchangers for side by side streams in one layer. However, the present work is highly significant to compute the rating requirements of plate fin heat exchangers for most helium liquefaction and refrigeration systems where effectiveness of heat exchangers is normally in excess of 0.95.

References

[1] Atrey MD. Thermodynamic analysis of Collins helium liquefaction cycle. Cryogenics 1998;38(12):1199–206.
[2] Shah RK, Sekulić DP. Fundamentals of heat exchanger design. New Jersey: John Wiley & Sons Inc.; 2003.
[3] Kakaç S, Liu H. Heat exchangers: selection, rating and thermal design. 2nd ed. London, New York: CRC Press; 2002.
[4] Smith EM. Advances in thermal design of heat exchangers a numerical approach: direct sizing, step-wise rating, and transients. John Wiley & Sons Limited; 2005.

[5] Kays WM, London AL. Compact heat exchangers. In: McGraw-Hill series in mechanical engineering. New York: McGraw-Hill Book Co; 1984.
[6] Kroeger PG. Performance deterioration in high effectiveness heat exchangers due to axial heat conduction effects. Adv Cryogenic Eng 1967;12:363–72.
[7] Chowdhury K, Sarangi S. Effect of finite thermal conductivity of the separating wall on the performance of counter flow heat exchangers. Cryogenics 1983;23(4):212–6.
[8] Narayanan SP, Venkatarathnam G. Performance degradation due to longitudinal heat conduction in very high NTU counterflow heat exchangers. Cryogenics 1998;38(9):927–30.
[9] Venkatarathnam G, Narayanan SP. Performance of a counter flow heat exchanger with longitudinal heat conduction through the wall separating the fluid streams from the environment. Cryogenics 1999;39(10):811–9.
[10] Ranganayakulu C, Seetharamu KN. The effects of longitudinal heat conduction in compact plate-fin and tube-fin heat exchangers using a finite element method. Int J Heat Mass Transfer 1997;40(6):1261–77.
[11] Chowdhury K, Sarangi S. Performance of cryogenic heat exchangers with heat leak from the surroundings. Adv Cryogenic Eng 1984;29:273–80.
[12] Barron RF. Effect of heat transfer from ambient on cryogenics heat exchanger performance. Adv Cryogenic Eng 1984;29:265–72.
[13] Gupta P, Atrey MD. Performance evaluation of counter flow heat exchangers considering the effect of heat in leak and longitudinal conduction for low-temperature applications. Cryogenics 2000;40(7):469–74.
[14] Chowdhury K, Sarangi S. The effect of variable specific heat of the working fluids on the performance of counter flow heat exchangers. Cryogenics 1984;24(12):679–80.
[15] Sahoo R, Sarangi S. Effect of temperature-dependent specific heat of the working fluid on the performance of cryogenic regenerators. Cryogenics 1985;25(10):583–90.
[16] Kumar KVR, Sarangi S. On the performance of high-N/tu heat exchangers with variable heat capacity of the working fluid. Heat Transfer Eng 1991;12(1):37–42.
[17] Soyars WM. The applicability of constant property analysis in cryogenic helium heat exchangers. Adv Cryogenic Eng 1991;37A:217–23.
[18] Mueller AC, Chiou JP. Review of various types of flow maldistribution in heat exchangers. Heat Transfer Eng 1988;9(2):36–50.
[19] Fleming RB. The effect of flow maldistribution in parallel channels of counter flow heat exchangers. Adv Cryogenic Eng 1967;12:352–62.
[20] Chowdhury K, Sarangi S. Effect of flow maldistribution on multipassage heat exchanger performance. Heat Transfer Eng 1985;6(4):45–54.
[21] Jung J, Jeong S. Effect of flow mal-distribution on effective NTU in multichannel counter-flow heat exchanger of single body. Cryogenics 2007;47(4):232–42.
[22] Pacio JC, Dorao CA. A review on heat exchanger thermal hydraulic models for cryogenic applications. Cryogenics 2011;51(7):366–79.
[23] Nellis GF. A heat exchanger model that includes axial conduction, parasitic heat loads, and property variations. Cryogenics 2003;43:523–38.
[24] Sorlie T. Three fluid heat exchanger design theory: counter and parallel flow. In: Technical report 54, Department of Mechanical Engineering, Stanford University, Stanford, CA; 1962.
[25] Aulds DD, Barron RF. Three-fluid heat exchanger effectiveness. Int J Heat Mass Transfer 1967;10:1457–62.
[26] Chato JC, Laverman RJ, Shah JM. Analyses of parallel flow multistream heat exchangers. Int J Heat Mass Transfer 1971;14(10):1691–703.
[27] Sekulić DP. A compact solution of the parallel flow three-fluid heat exchanger problem. Int J Heat Mass Transfer 1994;37(14):2183–7.
[28] Sekulić DP, Shah RK. Thermal design theory of three-fluid heat exchanger. Adv Heat Transfer 1995;26:219–328.
[29] Das PK, Ghosh I. Thermal design of multistream plate fin heat exchanger-a state of the art review. Heat Transfer Eng 2012;33(4–5):284–300.
[30] Haseler LE. Performance calculation methods for multistream plate-fin heat exchangers. In: Taborek J, Hewitt GF, Afgan N, editors. Heat exchangers: theory and practice. New York: Hemisphere/McGraw-Hill; 1983. p. 495–506.
[31] Prasad BSV, Gurukul SMKA. Differential method for sizing multistream plate fin heat exchangers. Cryogenics 1987;27:257–62.
[32] Prasad BSV, Gurukul SMKA. Differential methods for the performance prediction of multistream plate-fin heat exchangers. J Heat Transfer 1992 ;114(1):41–9.
[33] Kao S. A systematic design approach for a multistream exchanger with interconnected wall. In: ASME Paper 61-WA-255; 1961.
[34] Prasad BSV. The performance prediction of multistream plate-fin heat exchangers based on stacking pattern. Heat Transfer Eng 1991;12(4):58–70.
[35] Ghosh I, Sarangi SK, Das PK. An alternate algorithm for the analysis of multistream plate fin heat exchangers. Int J Heat Mass Transfer 2006;49: 2889–902.
[36] Ghosh I, Sarangi SK, Das PK. Simulation algorithm for multistream plate fin heat exchangers including axial conduction, heat leakage, and variable fluid property. J Heat Transfer 2007;129:884–93.
[37] Ghosh I, Sarangi SK, Das PK. Synthesis of multistream heat exchangers by thermally linked two-stream modules. Int J Heat Mass Transfer 2010;53: 1070–8.
[38] Wolf J. General solution of the equations of parallel flow multichannel heat exchangers. Int J Heat Mass Transfer 1964;7:901–19.
[39] Bentwich M. Multistream countercurrent heat exchangers. J Heat Transfer 1973;95(4):458–63.
[40] Prasad BSV. Fin efficiency and mechanisms of heat exchange through fins in multistream plate-fin heat exchangers: formulation. Int J Heat Mass Transfer 1996;39(2):419–28.
[41] Prasad BSV. Fin efficiency and mechanisms of heat exchange through fins in multistream plate-fin heat exchangers: development and application of a rating algorithm. Int J Heat Mass Transfer 1997;40(18):4279–88.
[42] Paffenbarger J. General computer analysis of multistream plate fin heat exchangers. In: Shah RK, Kraus AD, Metzger D, editors. Compact heat exchangers—a Festschrift for London AL. New York: Hemisphere; 1990. p. 727–46.
[43] Polley GT, Picon Nunez M. Methodology for the design of multistream plate-fin heat exchangers. In: Sunden B, Heggs PJ, editors. Recent advances in analysis of heat transfer for fin type surfaces. Ashurst Southampton: WIT Press; 2000. p. 251–76.
[44] Picon-Nunez M, Polley GT, Medina-Flores M. Thermal design of multistream heat exchangers. Appl Therm Eng 2002;22:1643–60.
[45] AspenONE. Aspen MUSE™, Version 2004.1, AspenTech India Pvt.
[46] Patankar SV. Numerical heat transfer and fluid flow. Hemisphere Publishing Corporation, McGraw-HILL Book Company; 1980.
[47] Users guide to GASPAK®, Version 3.35/3.45, Horizon Technologies; October 2007. <http://www.htess.com>.
[48] Users guide to HEPAK®, Version 3.40/ 3.41, Horizon Technologies; March 2005. <http://www.htess.com>.
[49] NIST Cryogenics Technologies Group. Material Properties. <http://cryogenics.nist.gov/MPropsMAY/materia/properties.html>.
[50] Manglik RM, Bergles AE. Heat transfer and pressure drop correlations for the rectangular offset strip fin compact heat exchanger. Exp Therm Fluid Sci 1995;10(2):171–80.